Evaluation of Hysteresis in Mercury Intrusion Porosimetry by Second-Intrusion Method

Ömer Z. Cebeci,* Middle East Technical University, Ankara, Turkey
T. Demirel and R. A. Lohnes, Department of Civil Engineering and Engineering
    Research Institute, Iowa State University

The theoretical basis of mercury intrusion porosimetry is reviewed, and the limitations of the Washburn equation as a means of converting the test data to a pore-size distribution curve are discussed. A procedure is suggested to distinguish the volume of pores with uniform radii from the volume of nonuniform or "ink-bottle" pores. The depressurization curve that results from reducing the pressure on mercury to allow retraction and ejection of mercury from the pores does not coincide with the pressurization curve. This hysteresis is attributed to the presence of ink-bottle or nonuniform pores. Physicochemical factors such as chemisorption and the difference in the contact angle of advancing and retreating mercury menisci contribute slightly to this hysteresis. Consideration of pore geometries demonstrates that the ejection pressure may not be equal to the intrusion pressure to a pore of given size. A comparison of the intrusion, depressurization, and reintrusion of two hypothetical samples illustrates the advantage of the second intrusion for interpreting pore-size distribution curves. The second intrusion gives the distribution of uniform pores and volumes of ink-bottle pores intruded at each entrance diameter. Finally, the second-intrusion method is applied to portland cement pastes with a 0.4 water-cement ratio that were hydrated for 3 and 60 d. It is observed that 60 to 64 percent of the porosity is in uniform pores that have a size distribution curve similar to the first-intrusion curve.

The theoretical basis for measuring the pore-size distribution of porous materials by intruding mercury into the pores was suggested by Washburn in 1921 ([1]). Ritter and Drake published the first experimental data in 1945 ([2]). Diamond applied this method to study of the evolution of porosity in hydrated portland cement pastes ([3]) and in 1970 introduced the concept for soil engineering applications ([4]). Very simply, this method involves evacuating the gases in the pores and then forcing mercury into the material by systematically increasing the pressure on mercury. Both the volume of mercury intruded and the pressure to achieve the intrusion are measured. The relation between the intrusion pressure P and the pore radius r is given by the Washburn equation ([1]):

$$P = -(2\gamma \cos \theta / r) \tag{1}$$

where γ is the surface tension of mercury and θ is the contact angle. From the data, it is possible to plot cumulative pore volume versus pore radius and thereby produce a pore-size distribution curve. This method assumes that all the pores are cylinders of uniform diameter and neglects the fact that, in cement pastes, soils, and other porous materials, they are irregular in shape and may be composed of large cavities interconnected by smaller necks. The pores with necks are referred to as "ink-bottle" pores.

Most mercury intrusion porosimeters have the capacity to reduce pressure after the maximum pressure has been reached and eventually to apply a vacuum so that the mercury in the pores is emptied. When this is done, the pressurizing curve does not coincide with the depressurizing curve. It is generally accepted that the hysteresis between the two curves is the result of some of the mercury being retained in the ink-bottle pores. Some preliminary interpretations regarding the pore structure of soils have

*Mr. Cebeci was with Iowa State University when this research was performed.

been made on the basis of the amount of mercury retained at the end of the depressurizing cycle ([4]).

The interpretation of mercury intrusion porosimetry data for a wide variety of materials is based on several approaches, and authors sometimes hold contradictory views on the exact procedure for interpreting the hysteresis ([2], [5], [6], [7], [8], [9], [10], [11], [12], [13], [14], [15]). The purpose of this paper is to unify these views and to suggest a procedure that can be followed to distinguish the volume of pores that have uniform radii from the volume of ink-bottle pores.

THEORY

The neck of an ink-bottle pore prevents the entry of mercury into the main portion of the pore at a pressure that corresponds to its radius according to Equation 1. Mercury intrudes an ink-bottle pore only when the applied pressure, as dictated by Equation 1, is high enough to enter the neck. During the depressurization phase, however, the mercury in the neck of the ink-bottle pore will be ejected (as explained later) at a pressure that corresponds to the collapse of the mercury column at the neck. The mercury in the main portion of the ink-bottle pore will thus be trapped and will not be ejected when the pressure reaches the level that favors its ejection because it has no contact with the mercury in the chamber. The total volume of mercury retained in the sample at the end of depressurization is thus a measure of the irregularity of the pore-size distribution; however, size distribution is not known for either the main portions or the necks of the pores. The depressurizing curve is difficult to interpret because several phenomena influence the shape of the curve.

A difference exists between the advancing and receding contact angles of mercury on the pore walls of the sample. The volume of mercury under the meniscus is greater under pressurization than under depressurization for pores of equal radii. Cooper ([14]) interprets this effect to be responsible for the hysteresis in mercury injection and ejection of silica samples.

Similarly, there is a difference between the advancing and receding contact angles of mercury on the sample cell. This is a small and constant effect throughout depressurization and can be corrected by making instrument adjustments at the start of depressurization.

The chemisorption of mercury on the pore walls of the sample results in mercury being retained in the sample and may be interpreted as mercury retained in ink-bottle pores. The amount of chemisorption depends on the surface properties of the sample.

Differences in the shapes of pores allow mercury to be ejected at different pressures. Various theoretical models have been developed by assuming idealized pore shapes to calculate ejection pressures. The pressure drop across the meniscus of mercury at the tip of an incompletely filled V-shaped pore causes ejection of the mercury immediately and continuously as the pressure is decreased.

If a cylindrical pore is completely filled, the meniscus does not exist, and the only force acting against the applied pressure is the adhesion tension between the surfaces of the pore wall and the mercury.

When the forces caused by these stresses are equal, the mercury is ejected. Hill (10) derived a theoretical equation for ejection pressure P_e and pore radius:

$$P_e = (\gamma \cos \theta / r) \qquad (2)$$

In comparing Equation 2 with Equation 1, it can be seen that mercury will be ejected from a completely filled cylindrical pore when the ejection pressure is half the pressure applied to penetrate the same pore. Hill (10) supports the validity of Equation 2 with experimental evidence obtained by intruding mercury into artificial pores of known diameter. When the mercury begins to collapse at the narrowest cross section of a nonuniform pore, the mercury column along the length of the pore that has a diameter equal to or less than twice the diameter of the narrowest section is ejected because the outside pressure is already reduced to the level that permits its ejection. Consequently, a "uniform cylindrical pore" is defined as a pore that has a cross section with a diameter range equal to or less than twice the diameter of its narrowest cross section; i.e., $r_{min} < r < 2r_{min}$, where r_{min} is the radius of the narrowest neck calculable by using Equation 2 and r represents the range of radius of a pore that is indistinguishable from a uniform pore with a constant radius of r_{min}.

A theoretical derivation similar to that used for cylindrical pores can be used to calculate the ejection pressure for rectangular pores. For a rectangular pore of width b and depth d (b > d), the ratio of penetration pressure to ejection pressure is $1 + d/b$. For slit-like pores where b is much greater than d, the ratio of penetration to ejection pressure should approach unity.

Several authors (5, 6, 7, 8, 13) have addressed the problem associated with toroidal volumes between spherical particles. At the end of penetration of mercury into an array of spheres, a volume of free space remains. This volume is a function of the packing of the spheres. If the pressure is decreased, the isolated mercury surfaces in the toroidal voids ultimately interfere and, at that moment, the retreating mercury sets free the entire pore space (5). This critical retraction pressure can be calculated for various types of packing.

The considerations discussed above illustrate the complexity of interpreting injection curves as well as hysteresis from mercury porosimetry. For pure clays, idealized models for rectangular pores may have some applicability, and pure granular soils in various states of compaction may be approximated by a toroidal model. But, for natural soils composed of both equidimensional particles and clay minerals, the pore geometry is very complex. The depressurizing curve is therefore limited to estimating the total volume of ink-bottle pores in the soil.

Another approach to the problem is to intrude the specimen a second time to determine the distribution of uniform pores. Hill (10) and Caro and Freeman (11) applied this technique, but they neglected to take the specimens out of the porosimeter before the second intrusion. Contamination of the stem walls of the sample cell by hydraulic fluid occurs during the first intrusion and results in errors in subsequent intrusion measurements. It is recommended that the sample cell be removed and the walls of the stem be cleaned before subsequent intrusions.

Of the factors mentioned above, chemisorption and contamination of the pore walls may affect the second-intrusion curve. Contamination of the pore walls of the specimen by mercury during the first intrusion might change the contact angle and thereby lead to errors in computations of pore size. Similarly, chemisorption might be misinterpreted as mercury retained in ink-bottle pores. These factors can be neglected because the second-intrusion method cannot detect small variations in pore sizes.

HYPOTHETICAL SPECIMENS

The intrusion, depressurization, and reintrusion of two hypothetical specimens are described here to illustrate how the second-intrusion method can improve the interpretation of the pore geometry of soils. Two hypothetical soil samples, designated s-1 and s-2, are shown in Figure 1(a). The two specimens have equal porosities and equal entrance diameters to all pores, but the shapes of two of the pores are different (for the purposes of discussion, the pores are numbered from 1 to 9). Thus, in Figure 1(a), pores 4 and 5 are of different shapes in the two specimens. All pores are cylindrical so that any vertical section through the specimen would result in the cross sections shown in Figures 1, 2, and 3. The tapered sections should not be visualized as cones but as cylinders of increasing or decreasing radii with very small heights. Again, for simplicity, the cross-sectional pore area rather than pore volume is discussed here. It is assumed that the pore distribution of these two specimens is measured by use of a porosimeter that has maximum pressure capacity for intruding pores down to a diameter of just larger than one unit. The mercury intrusion pore-size distribution curves of the two specimens will be identical, whereas the true pore-size distributions of the two specimens are in fact different.

Figure 1(a) shows the specimens surrounded by mercury in the sample cell. The specimens do not contain any large pores that would be intruded before the application of the first pressure increment. For convenience, mercury menisci are shown as straight lines rather than arcs in all subsequent figures. Fractions of pores 1 and 6 are filled when the pressure is increased to intrude pores of diameter equal to or greater than 6 units, as shown in Figure 1(b). Note that pores 8 and 9 in s-1 and pores 4, 5, 8, and 9 in s-2 have some portions that have diameters equal to or greater than 6 units but that they are not intruded at the corresponding pressures because of the narrower entrances into those sections. Figure 1(e) shows that pore 4 is completely filled when the pressure is high enough and a total area of 36 units is recorded to be in pores of diameter equal to 4 units. This is actually the case in s-1 whereas in s-2 the ink-bottle pore 4, with a main portion of maximum diameter of 9 units, is recorded as a uniform pore with a diameter of 4 units. Similar errors will occur as pores 5, 7, 8, and 9 are intruded [Figure 1(d) and (e)]. Parts of pointed tips of pores less than 1 unit in diameter (pore 1), small uniform pores such as pore 2, and larger ink-bottle pores with small necks such as pore 3 remain unintruded at the end of pressurization. Note that the cumulative first-intrusion curves for both specimens will be the same although the true pore-size distributions are different. The pore-size distribution curves are shown in Figures 4 and 5.

Figure 2(a) shows the early stages of depressurization. The pressure on mercury is released to the intrusion pressure of diameter equal to 3 units, and only the mercury surface in pore 1 is retracted to the level where the diameter is 3 units. There is no change in other pores. In Figure 2(b), the pressure is further released to the intrusion pressure of diameter equal to 4 units, and exactly at this point mercury columns in the parts of pores 7, 8, and 9 where the diameter is equal to 2 units collapse and the mercury is ejected from portions of these pores that have diameters equal to or smaller than 4 units at retreating menisci. From this point on, mercury in the main portions of pores 7 and 9 has lost con-

tact with the outside and thus will not respond to further decreases in the outside pressure. Figure 2(c) shows that, at a pressure equivalent to an intrusion diameter of 6 units (s-1), mercury from the main portion of pore 5, where the diameter is equal to 5 units, is ejected along with the entrance, where the diameter is equal to 3 units, because the variation in diameter is smaller than twofold. At this point, mercury at the entrances of pore 8 of both specimens and pore 5 of s-2 will collapse; thus, the mercury in those pores loses contact with the outside pressure and will not be ejected even though the pressure is further reduced. As depressurization continues, mercury in pores 4 and 6 will be ejected at the intrusion pressures of diameters equal to 8 units and 10 units respectively, but mercury will be retained at
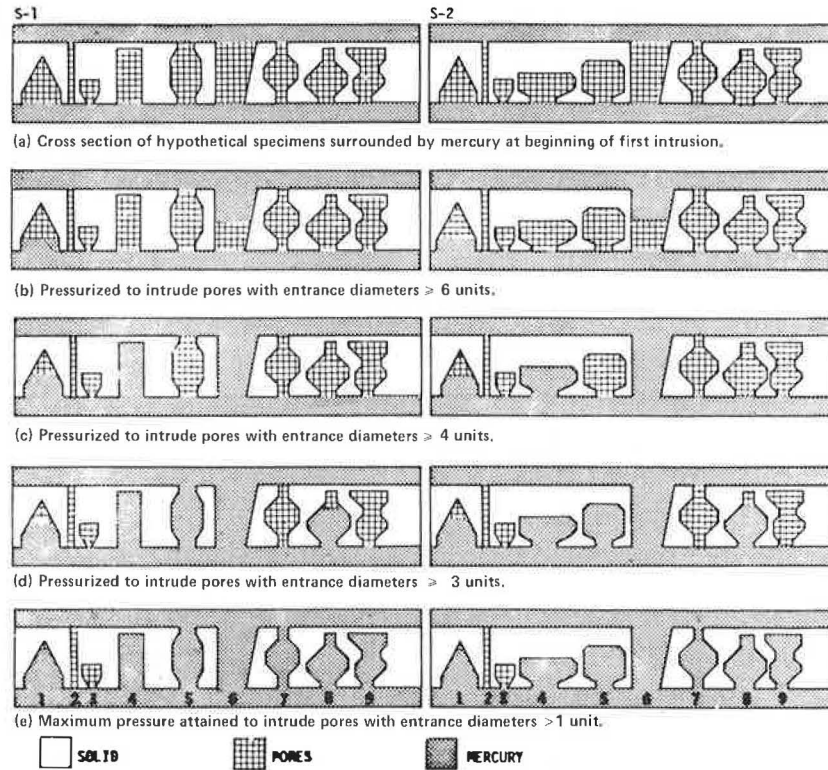
Figure 1. Schematic diagram of first intrusion.

(a) Cross section of hypothetical specimens surrounded by mercury at beginning of first intrusion.

(b) Pressurized to intrude pores with entrance diameters ≥ 6 units.

(c) Pressurized to intrude pores with entrance diameters ≥ 4 units.

(d) Pressurized to intrude pores with entrance diameters ≥ 3 units.

(e) Maximum pressure attained to intrude pores with entrance diameters >1 unit.

☐ SOLID   ▦ PORES   ▨ MERCURY

Figure 2. Schematic diagram of depressurization.

(a) Depressurized to the intrusion pressure of diameter = 3 units.

(b) Depressurized to the intrusion pressure of diameter = 4 units.

(c) Depressurized to the intrusion pressure of diameter = 6 units.

(d) Pressure released completely.

☐ SOLID   ▦ PORES   ▨ MERCURY
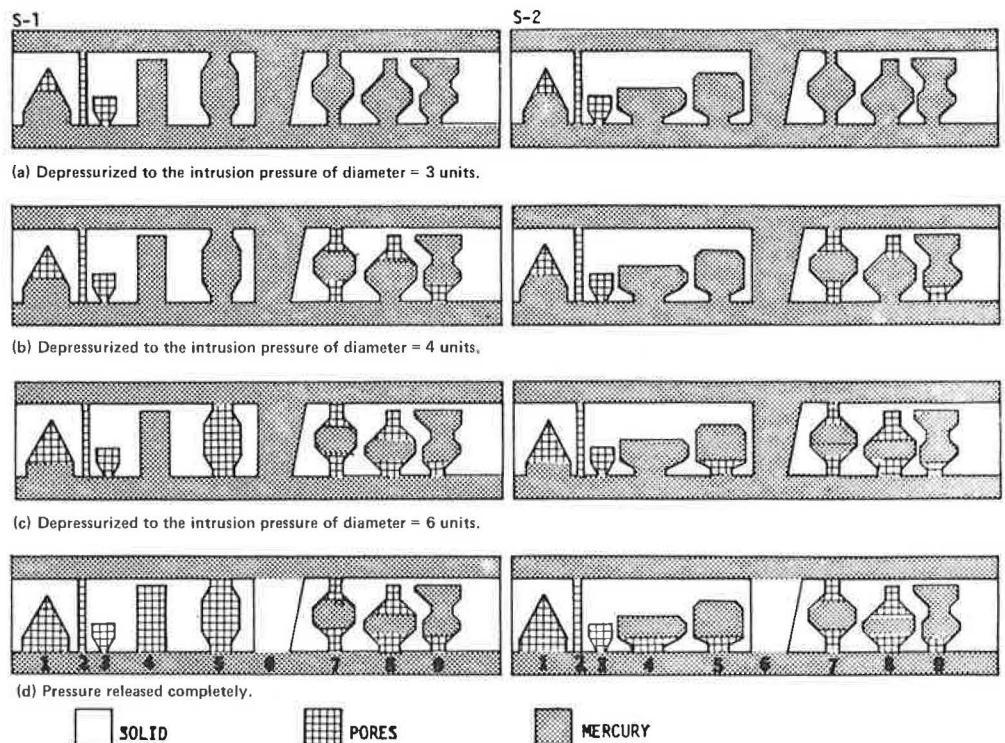
Figure 3. Schematic diagram of second intrusion.

(a) Pressurized to reintrude uniform pores with diameters > 6 units.

(b) Pressurized to reintrude uniform pores with diameters > 4 units.

(c) Pressurized to reintrude uniform pores with diameters > 3 units.

SOLID   PORES   MERCURY
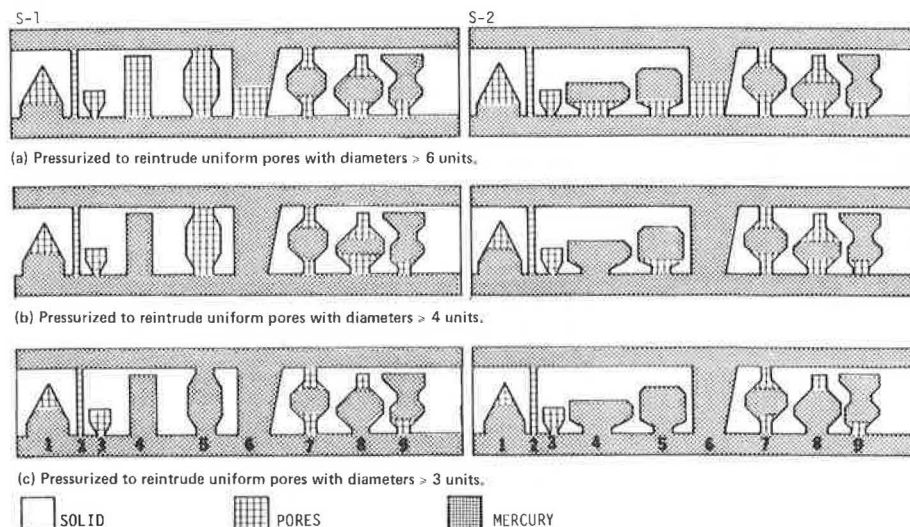
Figure 4. Pore-size distribution of hypothetical specimen s-1.

KEY:
○ ACTUAL PORE SIZE DISTRIBUTION
△ FIRST INTRUSION CURVE
□ SECOND INTRUSION CURVE
● INK-BOTTLE PORES
▲ DE-PRESSURIZATION CURVE
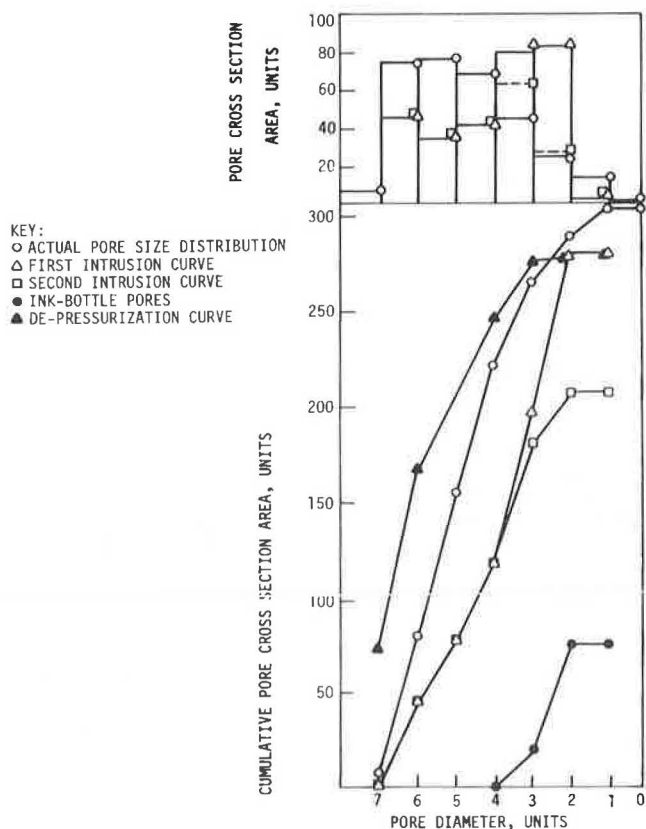
Figure 5. Pore-size distribution of hypothetical specimen s-2.

KEY:
○ ACTUAL PORE SIZE DISTRIBUTION
△ FIRST INTRUSION CURVE
□ SECOND INTRUSION CURVE
● INK-BOTTLE PORES
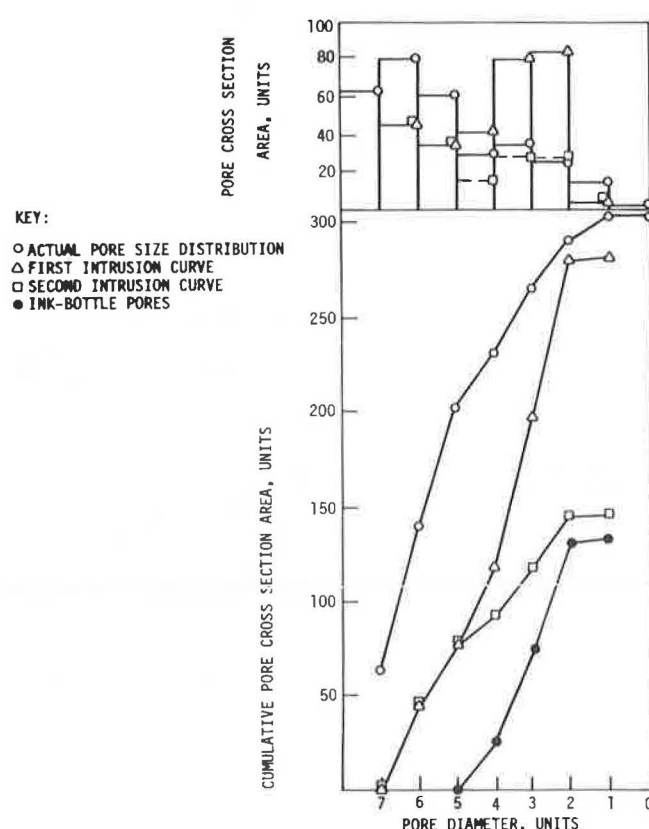
the portions of pore 4 of s-2 where the diameter is greater than 8 units. Figure 2(d) shows the end of the depressurization cycle. Mercury retained in s-1 and s-2 is 23.39 and 43.76 percent respectively of the true total pore cross-sectional areas. However, from porosimetry measurements, these percentages are observed as 25.36 and 47.45 percent respectively because of the unintruded pores.

Figure 3 shows the second-intrusion cycle where uniform pores and necks of ink-bottle pores are reintruded; the total intrusion is less than the first intrusion by the amount of mercury retained in the

sample at the end of depressurization. The final step of the second intrusion would be the same as that in Figure 1(e). The steps shown in Figures 1(e), 2, and 3 would be followed each time if pressurization and depressurization were repeated.

Pore-size distributions of the hypothetical specimens are shown in Figures 4 and 5. Chemisorption is neglected, and no alterations in the structure of the specimen are assumed. Contact angle of mercury and the specimen is assumed to be equal in the first and second intrusions. Obviously, the actual pore-size distributions cannot be determined by mercury intru-

Figure 6. Pore-size distribution of portland cement paste hydrated for 3 d.
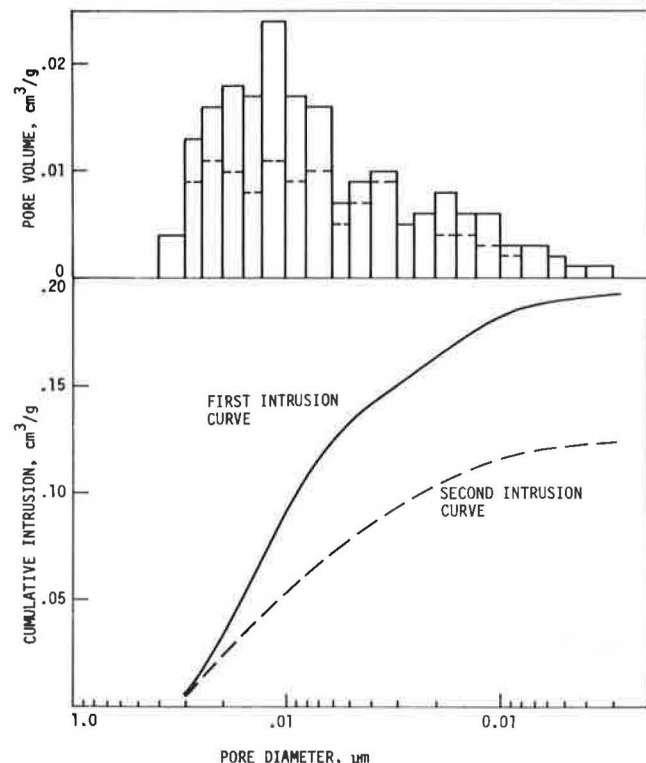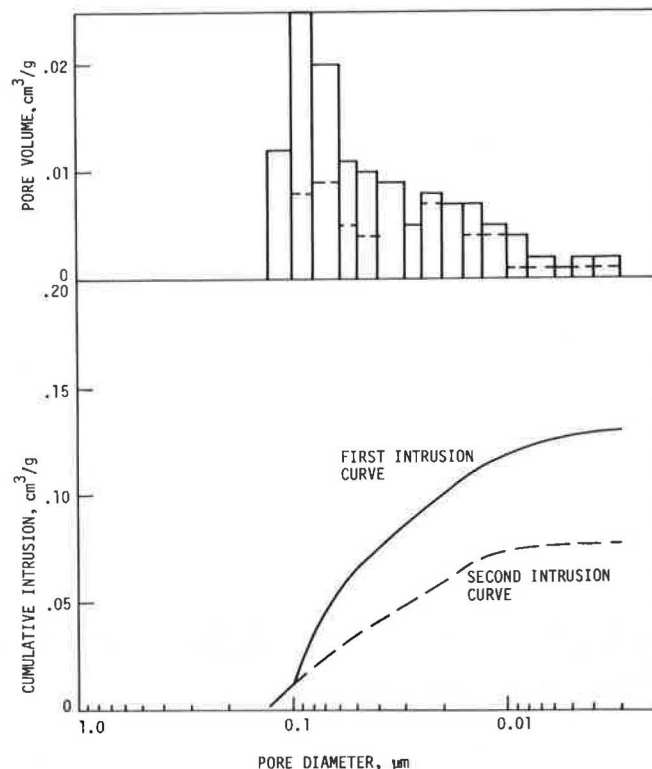

Figure 7. Pore-size distribution of portland cement paste hydrated for 60 d.

sion porosimetry although they are plotted in Figures 4 and 5 to show how closely the curves for first and second intrusions approach reality. The first-intrusion curve is the same for s-1 and s-2 but, by plotting the second-intrusion curve, the difference can be detected. It can then be concluded that both specimens have a total porosity of 279 unit squares (actually 302.5), but s-1 has 16.75 and 54 unit squares of ink-bottle pores with neck diameters of 3 and 2 units respectively, whereas s-2 has 26, 52, and 54 unit squares of ink-bottle pores with neck diameters of 4, 3, and 2 units respectively. Distribution of volume in ink-bottle pores intruded at each neck diameter can be plotted from the difference between first- and second-intrusion curves.

The conventional depressurization curve is plotted for s-1 in Figure 2(a). Note that the total amount of mercury retained in ink-bottle pores is the difference between the final points (diameters > 1 unit) of the first- and second-intrusion curves, which is also represented as the final point (diameter = 7 units) of the depressurization curve. In Figure 2(a), the large hysteresis between first-intrusion and depressurization curves reflects the fact that all pores are cylindrical and most are completely filled at the end of intrusion. If many pores had unfilled tips like pore 1 or were composed of slitlike shapes, the hysteresis loop would be smaller but the final point of depressurization would be the same.

The second-intrusion curves show that the distribution of uniform pores follows a pattern similar to that for the first-intrusion curve. The porosity of uniform pores decreases with increasing periods of curing time. The histograms in Figures 6 and 7 show that a large fraction of ink-bottle pores have entrance diameters slightly smaller than D_t, in which range the major portion of the total porosity of the pastes--both in uniform and ink-bottle pores--lies.

CONCLUSION

Evaluating hysteresis in mercury intrusion porosimetry by interpreting the depressurization curve is difficult because of the effect of interrelated physico-chemical phenomena that govern the ejection of mercury from various pore structures. Intruding the specimen a second time is suggested to distinguish the distribution of uniform pores from that of ink-bottles pores even though the exact pore-size distribution still cannot be obtained.

REFERENCES

1. E. W. Washburn. Note on a Method of Determining the Distribution of Pore Sizes in a Porous Material. Proc., National Academy of Sciences, Vol. 7, 1921, pp. 115-116.
2. H. L. Ritter and L. C. Drake. Pore Size Distribution in Porous Materials. Industrial and Engineering Chemistry, Analytical Ed., Vol. 17, 1945, pp. 782-786 and 786-791.
3. D. N. Winslow and S. Diamond. A Mercury Porosimetry Study of the Evolution of Porosity in Portland Cement. Journal of Materials, Vol. 5, 1970, pp. 564-585.
4. S. Diamond. Pore Size Distributions in Clays. Clays and Clay Minerals, Vol. 18, 1970, pp. 7-23.
5. S. Kruyer. The Penetration of Mercury and Capillary Condensation in Packed Spheres. Trans.,

Faraday Society, Vol. 54, 1958, pp. 1758-1767.

6. R. P. Mayer and R. A. Stowe. Mercury Porosime-try--Breakthrough Pressure for Penetration Be-tween Packed Spheres. Journal of Colloid Sci-ence, Vol. 20, 1965, pp. 893-911.

7. R. P. Mayer and R. A. Stowe. Mercury Porosimetry: Filling of Toroidal Void Volume Following Break-through Between Packed Spheres. Journal of Physi-cal Chemistry, Vol. 70, 1966, pp. 3867-3873.

8. H. I. Meyer. Pore Distribution in Porous Media. Journal of Applied Physics, Vol. 24, 1953, pp. 510-512.

9. A. Watson, J. O. May, and B. Butterworth. Studies of Pore Size Distribution. Trans., British Ceramic Society, Vol. 56, 1957, pp. 37-50.

10. R. D. Hill. A Study of Pore-Size Distribution. Trans., British Ceramic Society, Vol 59, 1960, pp. 198-212.

11. J. H. Caro and H. P. Freeman. Pore Structure of

Phosphate Rock and Triple Superphosphate. Jour-nal of Agricultural and Food Chemistry, Vol. 9, 1961, pp. 182-196.

12. R. G. Quynn. Internal Volume in Fibers. Textile Research Journal, Vol. 33, 1963, pp. 21-34.

13. L. K. Frevel and L. J. Kressley. Modifications in Mercury Porosimetry. Analytical Chemistry, Vol. 35, 1963, pp. 1492-1501.

14. A. R. Cooper. An Interpretation of Hysteresis Measurements in Mercury Porosimetry. American Chemical Society, Abstracts of Papers, Colloid and Surface Chemistry Section, Vol. 163, 1972.

15. L. A. De Wit and J. J. F. Scholten. Studies on Pore Structure of Adsorbents and Catalysts. Journal of Catalysis, Vol. 36, 1975, pp. 36-47.

Effects of Water Adsorption on Kaolin Clay During Shear

G. R. Glenn, Rutgers--The State University of New Jersey

Stress-controlled direct shear tests were made on laboratory-desiccated specimens of kaolin clay ($w_D \sim 1.5$ percent). The stan-dard apparatus was modified to permit progressive adsorption of water through the bottom porous plate. Various levels of constant shearing stress τ and a vertical stress of 24 kPa (3.5 lbf/in^2) were applied, and shearing deformation measurements to failure were taken. When the deformation rate accelerated markedly, failure was defined for that particular τ and water content w. Failure sur-face w determinations were confirmed by an independent study of time versus wetting rate. Deceleration in wetting rate with increas-ing water content indicated decreasing negative pore pressure or soil water suction. Suction increases shearing resistance by its "re-inforcement" of effective normal stress between soil solids; it is greater at lower w and reduces most at w > 23 percent—the point of contraflexure in the wetting rate versus w curve—which is fol-lowed by swelling. Higher constant stress levels produced initial de-formations at lower w and at higher deformation rates. The ap-proximately linear relation between applied τ and w at initial de-formation indicates that increases in w account for decreases in in-terparticle shearing resistance and corresponding losses of strength. This is confirmed by qualitative analysis of test results in relation to the Coulomb equation and the principle of effective stress. Be-cause the maximum strength of specimens at w_D was greater than maximum strengths between 1.5 and 23 percent, stress-controlled tests were replaced by strain-controlled tests; therefore, peak and residual strengths were obtained on desiccated specimens rewet to w in this range and held constant during stress application. These tests were extended to w_E (equilibrium w ~ 35 percent) for com-parison with stress-controlled test results.

Most of the available laboratory test data on strength and strain in soils have been obtained over relatively short periods of time, generally from a few minutes to a few hours. However, in field situations, long-term loads maintain stress for years and have been observed to produce continuing small strains. This phenomenon, known as "creep," occurs in soils under sustained high stress, normally without change in water content w. Many environmental factors affect

soil response but are difficult to identify. High on any list of the causes of the instability of clays in relation to decrease in strength are adsorption of water and resultant swelling, pore water pressure, and strain. Thus, the most obvious and perhaps most significant of the environmental factors is water; its effects are increased shearing deformation or creep accompanied by loss of shearing strength.

As the ratio of shearing resistance to applied shearing stress for the potential failure surface ap-proaches unity, the specimen approaches failure. As soon as the applied stress becomes about half the peak value, the clay is likely to deform or creep at constant shearing stress (1). The typical plot of deformation as a function of time indicates higher rates for higher constant stress levels; failure is indicated by a markedly rapid increase in deformation rate and a simultaneous decrease in stress.

The contributing factors to shearing resistance of soil are related in the following form of the Coulomb equation:

$$\tau_{ff} = \bar{c} + \bar{\sigma}_{ff} \tan \bar{\phi} \tag{1}$$

where τ_{ff} is peak shearing strength, which is known to depend on the effective stress in the soil (sub-scripts ff indicate "on the failure plane at failure").

The angle of internal friction $\bar{\phi}$, measured as the slope of the Mohr strength envelope, based on effec-tive stresses, varies from zero for a saturated clay to about 30.9 for some fairly dry clays; $\bar{c}$, the cohe-sion or the minimum shear strength exhibited by the clay at zero normal stress, is measured as the inter-cept of the Mohr envelope on the shear axis. For partially saturated clay, τ_{ff} increases with increas-ing effective normal stress $\bar{\sigma}_{ff}$ on the failure plane at failure. The original Terzaghi equation for ef-fective stress in fully saturated soils (1) provides the understanding of the principle and is expressed as